Supporting Information

Green Synthesis of Manganese-Based Anti-Perovskite with Anti-Thermal Quenching Properties for LED

Siyuan Chen[a,b†], Wangqi Mao[b†*], Yaohua Jiang[d], Yang Liu[e], Jingzhou Li[c], Chi Zhang[c], Hao He[a*], Hongxing Dong[b,c*], and Long Zhang[b,c]

S1: Rietveld refinement analysis of the samples prepared with and without $C_2H_2O_4$.

Rietveld refinement was performed to quantitatively analyze the phase composition of the samples prepared with and without oxalic acid. The refinement included CsBr, Cs_3MnBr_5 ($[MnBr_4]BrCs_3$), and $Cs_2MnBr_4(H_2O)_2$ phases, corresponding to residual CsBr, the tetrahedrally coordinated manganese bromide phase, and the octahedrally coordinated hydrated manganese bromide phase, respectively. The observed, calculated, and difference patterns, together with the Bragg positions, are shown in Fig. S1. The refined phase fractions, PDF IDs, space groups, lattice parameters, and fitting indices are summarized in Table S1.

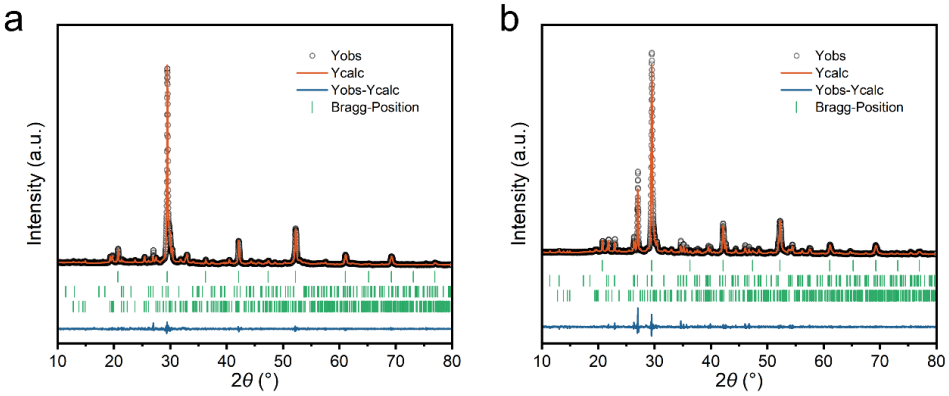

Fig. S1. Rietveld refinement profiles of the samples prepared (a) without $C_2H_2O_4$ and (b) with $C_2H_2O_4$. The observed, calculated, and difference patterns are shown together with the Bragg positions of CsBr, Cs_3MnBr_5, and $Cs_2MnBr_4(H_2O)_2$.

Table S1. Rietveld refinement results of the samples prepared without and with $C_2H_2O_4$.

Chemical formula		**CsBr**	**Cs_3MnBr_5**	**$Cs_2MnBr_4(H_2O)_2$**
Without $C_2H_2O_4$				
Relative content (wt.)		70.966%	3.275%	25.759%
PDF ID#		98-005-3848	01-071-1416	00-050-0630
Space groups		Pm-3m	I4/m cm	P-1
Lattice parameters	a(Å)	4.287564	9.645972	5.980358
	b(Å)	4.287564	9.645972	7.06404
	c(Å)	4.287564	15.447928	7.581704
	α(°)	90	90	65.9997
	β(°)	90	90	87.8872
	γ(°)	90	90	83.9921
	Volume	78.819	1437.349	290.988

Fit indices		Rp: 2.87% Rwp: 3.769% Chi2: 0.48		
With $C_2H_2O_4$				
Relative content (wt.)		27.525%	35.596%	36.879%
PDF ID#		98-005-3848	01-071-1416	00-050-0630
Space groups		Pm-3m	I4/m cm	P-1
Lattice parameters	a(Å)	4.289983	9.600524	5.966499
	b(Å)	4.289983	9.600524	7.060556
	c(Å)	4.289983	15.552286	7.603826
	α(°)	90	90	65.8739
	β(°)	90	90	87.9142
	γ(°)	90	90	84.0218
	Volume	78.953	1433.455	290.747
Fit indices		Rp: 3.30% Rwp: 4.491% Chi2: 0.91		

S2: Crystal structure of $[MnBr_4]BrCs_3$.

The crystal structure of $[MnBr_4]BrCs_3$ is shown in Fig. S2. The isolated $[MnBr_4]$ tetrahedra are surrounded by a three-dimensional anti-perovskite framework formed by corner-sharing $[BrCs_6]$ octahedra. Such spatially separated $[MnBr4]^{2-}$ luminescent centers can reduce the interaction between neighboring Mn^{2+} centers and are beneficial for achieving stable green emission.

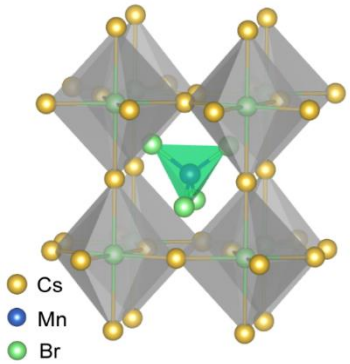

Fig. S2. Crystal structure of $[MnBr_4]BrCs_3$. The isolated $[MnBr_4]$ tetrahedra are surrounded by a three-dimensional anti-perovskite framework formed by corner-sharing $[BrCs_6]$ octahedra.

S3: FTIR analysis of MnBr precursor powders prepared with and without $C_2H_2O_4$.

FTIR spectra of the MnBr precursor powders prepared with and without oxalic acid were collected to further clarify the interaction between oxalic acid/oxalate groups and Mn^{2+} centers. As shown in Fig. S3, the MnBr precursor powder prepared without oxalic acid shows weak vibration bands, including O–H stretching around 3387 cm^{-1}, H–O–H bending around 1611 cm^{-1}, Mn–OH/Mn–O-related vibrations at 1315 and 787 cm^{-1}, and a Mn–Br-related lattice vibration around 493 cm^{-1}.

After oxalic acid treatment, new oxalic-acid/oxalate-related vibration bands appear at 1594, 1035, 869, and 677 cm^{-1}, which can be assigned to COO− stretching, C–C stretching, and O–C=O bending vibrations. Meanwhile, the Mn–Br-related vibration shifts from 493 to 538 cm^{-1} after oxalic acid treatment. These

spectral changes suggest that oxalic acid/oxalate interacts with Mn^{2+} centers and modifies the local coordination environment of the Mn-containing precursor species.

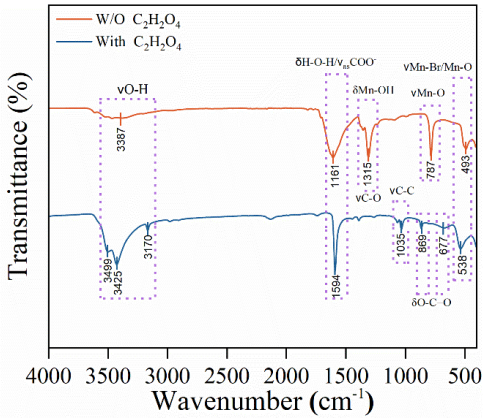

Fig. S3. FTIR spectra of MnBr precursor powders prepared with and without $C_2H_2O_4$. The spectra are vertically shifted for clarity.

S4: Power-dependent spectra of $[MnBr_4]BrCs_3$ excited by a 405 nm CW laser.

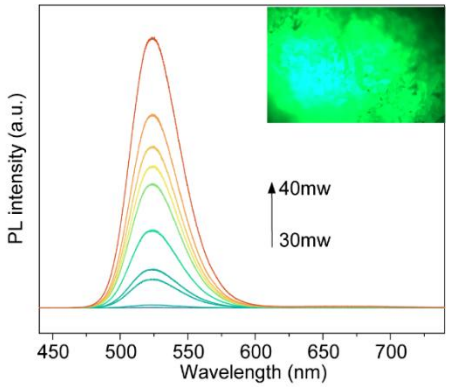

Fig. S4. Power-dependent PL spectra of $[MnBr_4]BrCs_3$ excited by a 405 nm CW laser.

S5: PL spectrum of prepared $[MnBr_4]BrCs_3$ with and without oxalic acid during synthesis.

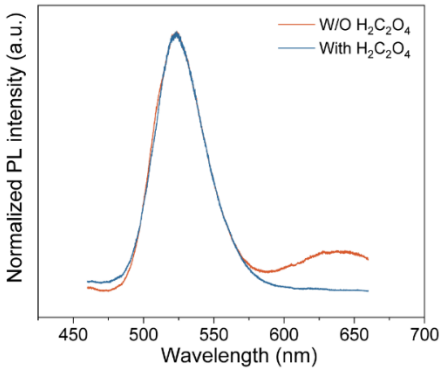

Fig. S5. PL spectrum of prepared $[MnBr_4]BrCs_3$ with and without oxalic acid during synthesis.

S6. Absolute PLQY of $[MnBr_4]BrCs_3$ prepared with and without oxalic acid.

The absolute photoluminescence quantum yield (PLQY) of $[MnBr_4]BrCs_3$ powder samples was measured at room temperature in ambient air under 365 nm excitation using an integrating sphere. As shown in Fig. S6, the $[MnBr_4]BrCs_3$ sample prepared with oxalic acid exhibits an absolute PLQY of 60.81%, whereas the sample prepared without oxalic acid shows a much lower PLQY of 20.64%. The significantly enhanced PLQY further confirms the important role of oxalic acid in improving the luminescence efficiency of the manganese-based anti-perovskite.

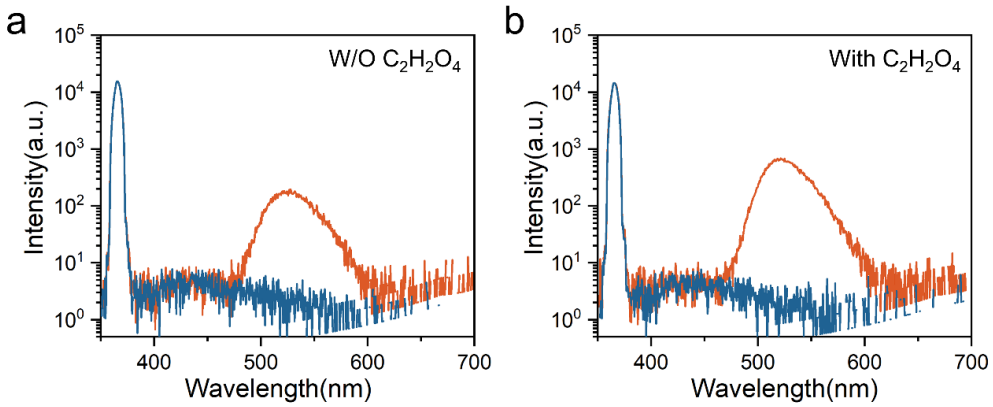

Fig. S6. Absolute PLQY spectra of $[MnBr_4]BrCs_3$ prepared (a) without oxalic acid and (b) with oxalic acid under 365 nm excitation. The corresponding PLQY values are 20.64% and 60.81%, respectively.

S7: Pseudocolor mapping of temperature-dependent PL spectra from 397 K to 497K.

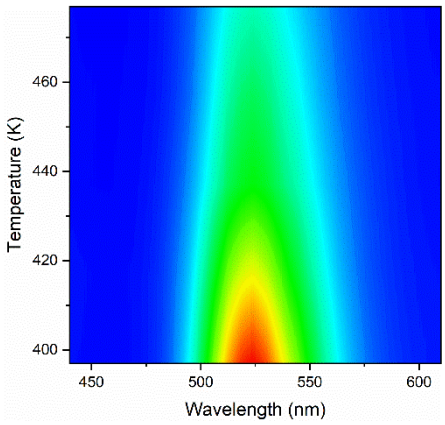

Fig. S7. Pseudocolor mapping of temperature-dependent PL spectra from 397 K to 497 K

S8: Arrhenius-type analysis of temperature-dependent PL lifetime.

An Arrhenius-type analysis was performed to further evaluate the temperature-dependent emission dynamics of $[MnBr_4]BrCs_3$. Based on the fitted PL lifetimes obtained from the temperature-dependent decay curves, $\ln(1/\tau)$ was plotted as a function of $1/T$, where τ is the fitted PL lifetime at each temperature. As shown in Fig. S8, the linear fitting gives an apparent activation energy of approximately 5.6 meV, suggesting that a low-barrier thermally activated process is involved in the temperature-dependent emission dynamics.

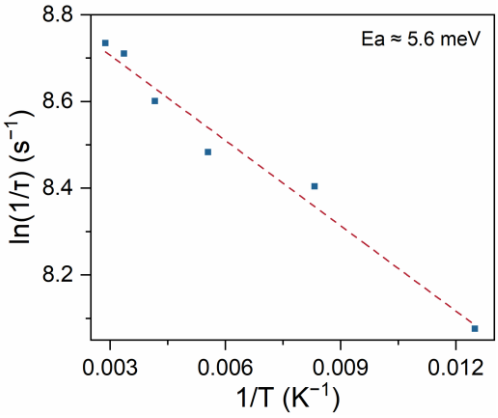

Fig. S8. Arrhenius-type plot of ln(1/τ) versus 1/T based on the temperature-dependent PL lifetimes of $[MnBr_4]BrCs_3$. The dashed line represents the linear fit, giving an apparent activation energy of approximately 5.6 meV.

S9: Stability measurements of $[MnBr_4]BrCs_3$.

Integrated emission intensity of $[MnBr_4]BrCs_3$ was measured under continuous 405 nm CW laser excitation at a constant pump power of 40 mW in ambient air. As shown in Fig. S9a, the material maintains its PL output without severe degradation during continuous laser irradiation, showing a half-life of approximately 12 h. In addition, the storage stability of the powder samples prepared with and without oxalic acid was evaluated under ambient conditions. As shown in Fig. S9b, the samples were photographed under daylight and 365 nm UV light after storage in ambient air for 1, 5, 10, 15, and 20 days. The oxalic-acid-assisted sample still exhibits bright green emission after 20 days, indicating good storage stability under ambient conditions.

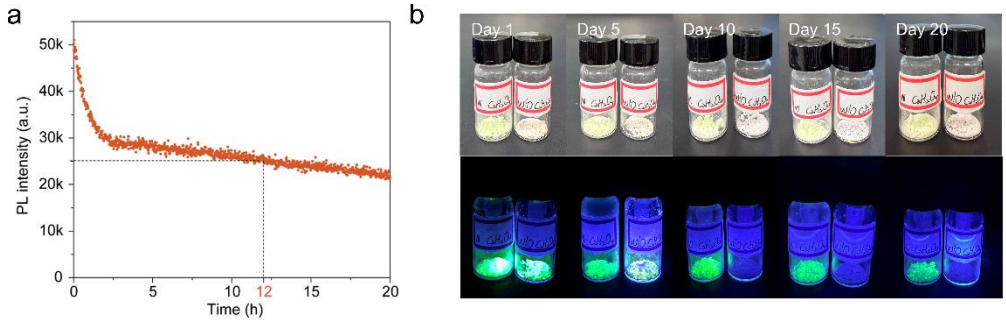

Fig. S9. Stability measurements of $[MnBr_4]BrCs_3$.

S10. Comparison of this work with representative Mn-based green-emitting halides in terms of synthesis route, environmental aspect, optical performance, stability, and device metrics.

Table S2. Comparison of this work with representative Mn-based green-emitting halides in terms of synthesis route, environmental aspect, optical performance, stability, and device metrics.

Material	Synthesis / environmental aspect	λ_{em} / FWHM	PLQY	Stability / device	Key gap vs this work

This work: $[MnBr_4]BrCs_3$	**Water-based evaporation; Lead-free**	**524 nm / 41 nm**	**60.81%**	**anti-thermal-quenching; UV-pumped LED, 257445 cd/m^2, T50 = 870 min**	-
Su et al. 2019, Cs_3MnBr_5	high-temperature phosphor synthesis; lead-free	520 nm / 42 nm	49%	423 K retention: 82%; pc-WLED, 107.76 lm/W	requires organic solvents; more complex process;
Kong et al. 2021, Cs_3MnBr_5 NCs	hot-injection; lead-free; organic-solution-based	green / 43 nm	48%	humidity-triggered phase change	requires organic solvents ; more complex process
Bao et al. 2025, Cs_3MnBr_5	water evaporation; lead-free; no organic solvent/ligand	523–524 nm / —	58%	10-loop retention: 87%; UV-LED demo	no explicit anti-thermal-quenching
Li et al. 2023, Cs_3MnBr_5	glass crystallization; lead-free	524 nm / 47 nm	60.2%	10 h retention: ~94%; green LED, EQE 8.5%	glass-assisted route; more complex process ; broader emission
Zhang et al. 2023, $(BPTP)_2MnBr_4$	solvent–antisolvent recrystallization; hybrid system	515 nm / 43 nm	82%	393 K retention: 79%; white LED, 112 lm/W	requires organic solvents; hybrid material
Yoo et al. 2024, Cs_3MnBr_5	modified hot-injection; lead-free all-inorganic	~520 nm / 41.5 nm	60%	color-conversion film; photodetector	requires organic solvents; more complex process;

Table S2 shows that the present work is distinguished from representative Mn-based green emitters by its nontoxic water-based synthesis, narrow-band green emission (524 nm, ~41 nm), explicit anti-thermal-quenching behavior, and UV-pumped LED performance. While some reported systems exhibit higher PLQY or stronger device metrics, they often involve more complex processing, organic-solvent-based routes, hybrid compositions, or encapsulation-assisted strategies.